In vivo deuterated water labeling followed by deuterium magnetic resonance imaging of xenografted tumors.

Julian C. Assmann[1], Jeffrey R. Brender[2], Don E. Farthing[1], Keita Saito[2], Kathrynne A. Warrick[1], Natella Maglakelidze[1], Hellmut Merkle[3], Murali C. Krishna[2], Ronald E. Gress[1], Nataliya P. Buxbaum[1*]

[1]Experimental Transplantation and Immunology Branch, National Cancer Institute, National Institutes of Health, Bethesda, Maryland, USA
[2]Radiation Biology Branch, Center for Cancer Research, National Cancer Institute, National Institutes of Health, Bethesda, Maryland, USA
[3]Laboratory for Functional and Molecular Imaging, National Institute of Neurological Disorders and Stroke, National Institutes of Health, Bethesda, Maryland, USA

[*]Corresponding author:
Nataliya P. Buxbaum, M.D., Experimental Transplantation and Immunology Branch, National Cancer Institute, Bethesda, Maryland, USA, Email: nbuxbaum@mail.nih.gov

Abstract

In vivo deuterated water (^2H_2O) labeling leads to deuterium (^2H) incorporation into biomolecules of proliferating cells and provides the basis for its use in cell kinetics research. We hypothesized that rapidly proliferating cancer cells would become preferentially labeled with ^2H and, therefore, could be visualized by deuterium magnetic resonance imaging (dMRI) following a short *in vivo* ^2H_2O labeling period. We initiated systemic ^2H_2O labeling in an HT-29 xenograft model and performed dMRI following 7 and 14 days of *in vivo* tumor growth and labeling. We show that small tumors, not otherwise distinct from normal tissue by anatomical MRI, were readily apparent on dMRI following 7 days of labeling. This novel labeling-imaging approach allows safe and nonradioactive, *in vivo* detection of cancer. Our method could be well suited for clinical settings that require serial imaging where repeated exposure to radiotracers should be avoided.

Keywords: deuterium, magnetic resonance spectroscopy, cancer imaging, metabolism

Introduction

Imaging is an essential tool for cancer diagnosis, staging, and surveillance. Positron emission tomography and computer tomography (PET-CT) scans are commonly used in this setting. They provide clinically valuable information that can guide therapeutic decisions[1-3]. Radioactive tracers, such as ^{18}fluorodeoxyglucose (FDG), in combination with CT take advantage of unique features of cancer cells such as their highly proliferative and glycolytic nature, allowing identification of small tumors that are not detectable by anatomical imaging alone[4]. Such detection can result in clinically meaningful outcomes for patients, as surgical or medical interventions can be undertaken at lower tumor burden, i.e. prior to local growth and/or metastasis.

However, PET-CT scans can expose patients to an increasing amount of radiation, especially when used serially as is often the case in the setting of cancer screening or surveillance (e.g. familiar predisposition syndromes), measuring treatment responses, or monitoring for disease recurrence or relapse[5]. In recent years, the increasing use of PET-CT scans and other medical procedures that require the use of radiation has led to a 33% increase in medical procedure-related radiation exposure in the US population[6]. In addition, some tumors are not highly FDG-avid, and certain tissues or anatomical locations are not amenable to imaging using FDG as a tracer[7]. For instance, high renal clearance of FDG limits its utility in kidney neoplasms, and brain tumors are difficult to distinguish from normal brain parenchyma due to the high baseline glucose utilization in the brain[8].

While the amount of radioactivity per individual dose of a radiotracer administered for PET-CT is small, a nonradioactive equivalent would be of great value. Nonradioactive alternatives to PET-CT are currently being developed, mainly in combination with magnetic resonance imaging (MRI). This includes hyperpolarized ^{13}C-MRI, a technique that uses dynamic nuclear polarization (DNP) to facilitate detection of ^{13}C-labeled substrates (e.g. ^{13}C-pyruvate)[9]. Despite its ability to elucidate *in vivo* metabolism in preclinical and clinical settings, its expense and complex logistics may hinder its wide clinical applicability[10-12]. In addition to ^{13}C, substrates labeled with deuterium (^{2}H), have recently been explored for visualization of aberrant tumor metabolism[13,14].

We hypothesized that, instead of using a labeled tracer, we would be able to preferentially label tumor cells *in vivo* by providing deuterated water ($^{2}H_2O$) systemically for a short period of time. By definition, tumor cells exhibit rapid growth and frequent cell division. To sustain these high rates of proliferation, cells must generate new cellular biomass[15,16]. During biosynthesis, (deuterated) water can be used as a substrate for enzymatic reactions in multiple pathways, leading to the formation of stable carbon-deuterium bonds that are not exchangeable with hydrogen, thus allowing *in vivo* labeling of proliferating cells with simple oral administration of deuterated water[17-19]. This principle has formed the basis for a decades-long use of deuterated water to study cell cycle kinetics in both patients and animal models with virtually no adverse effects reported at low to moderate concentrations (up to 20-30% v/v) in animal studies[20-22].
We recently applied deuterium MRI (dMRI) to visualize target organs of graft-versus-host disease infiltrated by alloreactive T cells, which share certain features with tumor cells, i.e. rapid proliferation and glycolytic metabolism[22].

Here, we present a novel imaging approach using *in vivo* $^{2}H_2O$ labeling followed by dMRI for the visualization of tumors in a xenograft mouse model. Using this deuterium administration protocol with tumor-bearing mice, we quantitatively show by mass spectrometric analysis that tumor xenografts undergo a concentration-dependent enrichment of deuterium in the DNA base deoxyadenosine (dA). By combining deuterium labeling with dMRI, we successfully visualized small tumors (<1 cm in diameter) that were not distinguishable from normal tissue by proton MRI in a xenograft model, demonstrating the ability of this technique to detect small tumors without the use of radioactivity. This relatively easy to implement, non-radioactive imaging technique could provide a useful addition to the imaging armentarium in cancer research.

Results

$^{2}H_2O$ uptake leads to a dose-dependent increase of isotopologically labeled deoxyadenosine in tumor cells

Water is a substrate for multiple biosynthetic pathways required for cell proliferation, including amino acid (proteins, peptides), nucleic acid (DNA, RNA), and fatty acid (lipids) synthesis (Fig. 1a). When deuterated water is administered systemically, biomolecules within rapidly proliferating cells incorporate deuterium; hence, deuterium enrichment can serve as a proxy for cell proliferation[17,18,22-25]. Using a quantitative gas chromatography tandem mass spectrometry (GC-MS/MS) method, we measured deuterium enrichment into dA of xenografted tumors[22,26,27]. To accomplish this, we injected one million human HT-29 adenocarcinoma cells into the hind limbs of athymic Foxn1^{nu} mice and quantified dA isotopologues (M+1, M+2, M+3, and M+4) in the resultant tumors following 7 and 14 days of *in vivo* tumor growth during concurrent $^{2}H_2O$ labeling. The contralateral hind limb was not injected with HT-29 cells, and a small section of the quadriceps muscle from that limb was excised to serve as negative control tissue for the GC-MS/MS analysis. In addition, we collected a urine or serum sample from each study animal on the day of imaging to measure total body water (TBW) deuterium enrichment via headspace (HS)-GC-MS[27], which was confirmed to be ~6-9% for all animals that underwent imaging.

The natural isotopic background in deoxyadenosine (dA), resulting mainly from the natural abundance of ^{2}H, ^{13}C, ^{15}N and ^{17}O, ranges from 23% to 26% in both tumor without $^{2}H_2O$ labeling and muscle tissue (Fig. 1b). Deoxyadenosine extracted and purified from the tumors of mice receiving maintenance deuterated water of increasing concentrations (0%, 8%, 16% and 32%) showed a dose-dependent linear increase in isotopologue enrichment of dA.

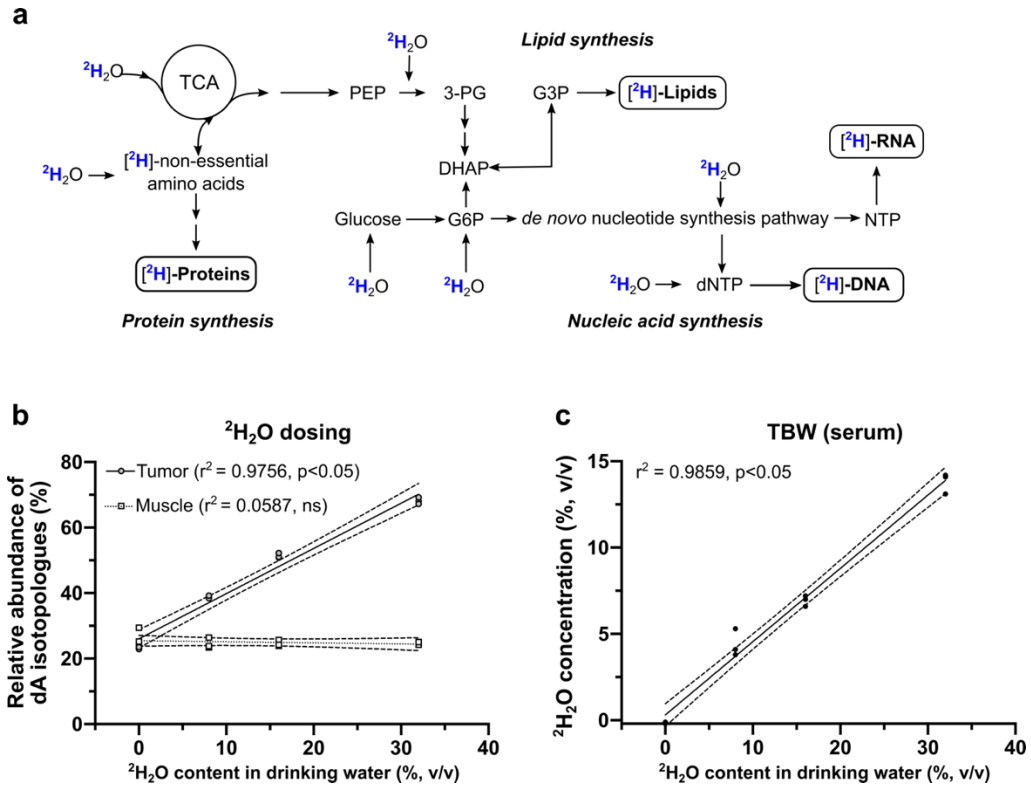

Figure 1: ^2H_2O is incorporated into biomolecules and leads to a dose-dependent increase in the isotopologue abundance of dA. a) *Schematic illustration of biosynthetic pathways in a cell that utilize water and are therefore possible routes for nonexchangeable, stable deuterium incorporation into carbon-deuterium bonds. PEP, phosphoenolpyruvate; 3-PG, 3-phosphoglycerate; DHAP, dihydroacetone-phosphate; G6P, glucose-6-phosphate; G3P, glycerol-3-phosphate; (d)NTP, (deoxy)nucleoside triphosphate.* ***b)*** *Dose-dependent increase of dA isotopologue abundance (dA m+1, m+2, m+3, m+4 and m+5). Mice were injected with human HT-29 adenocarcinoma tumor cells ($1x10^6$) in the right hind limb and labeled with increasing concentrations of ^2H_2O by injection of up to four i.p. boluses (35 ml/kg, 0.9% NaCl in 100% ^2H_2O) followed by the administration of ^2H_2O in drinking water for maintenance dosing (0-32%, v/v). Two weeks after tumor cell implantation, the tumors as well as muscle tissue of the contralateral hind limb serving as a negative control were excised. The DNA was isolated and dA isotopologue abundance was quantified via GC-MS/MS. Statistical testing was performed using linear regression (n=3 per group).* ***c)*** *The ^2H_2O concentration in total body water was quantified using serum samples collected via mandibular or retroorbital bleed after a two-week labeling period with increasing concentrations of ^2H_2O. The quantification was carried out using a headspace GC-MS method and statistically tested using linear regression (n=3 per group).*

This increase in dA isotopologue enrichment above natural isotopic background was not detected in muscle tissue of the contralateral leg (Fig. 1b). Metabolic labeling of cellular biomass with 8% ^2H_2O as maintenance dose (in drinking water) resulted in ~5% ^2H_2O in TBW and a tumor deuterium enrichment of 38.7% ± 0.2 after two weeks of labeling (Fig. 1b, c). Higher maintenance doses of ^2H_2O led to an increased TBW and tumor dA enrichment, i.e. 16% ^2H_2O resulted in ~7% TBW and 51.3% ± 0.4 dA isotopologue enrichment and 32% ^2H_2O resulted in ~14% TBW and 68.2% ± 0.6 dA isotopologue enrichment, respectively (Fig. 1b, c). Meanwhile, the isotopologue enrichment of dA isolated from the contralateral muscle tissue (control) remained stable at around 24% for the full range of tested TBW ^2H_2O concentrations (Fig. 1b), confirming that ^2H_2O preferentially labeled tumor cells. The drinking water was tested upon completion of the study and was confirmed to be the targeted ^2H_2O concentration (Supplementary Fig. 1a). Importantly, we found that the use of 8%, 16%, and 32% ^2H_2O in drinking water led to multiple deuterium atoms

being incorporated into the dA molecule, with more than half of dA molecules containing more than one deuterium atom (e.g. dA M+2, M+3, Supplementary Fig. 1b). Although we can reliably quantify the deuterium enrichment via mass spectrometry, the analysis is carried out *ex vivo* and requires a tissue sample. In a clinical setting, acquiring tissue biopsies can be difficult and there are situations where the tumor is inaccessible, or the biopsy is otherwise medically inadvisable.

In addition to clinical contraindications for biopsy, the heterogeneity and variability in metabolic activity within a tumor may result in inconsistent deuterium quantification depending on the specific region sampled[28,29]. Due to these limitations, we pursued the development of an imaging modality that would circumvent the clinical risks and potential sampling error of the biopsy approach. We hypothesized that *in vivo* imaging of deuterium following biosynthetic labeling would allow noninvasive detection and monitoring of molecular pathways distinct from those visualized with current techniques such as FDG-PET or hyperpolarized ^{13}C-MRI. DNA itself is unlikely to be detected via MRI due to its short T2 and long T1 relaxation rates stemming from its size and relative stiffness. However, other metabolic intermediates enriched with deuterium may be detected, if they accumulate within the tumor in sufficient abundance[30,31]. We therefore set out to evaluate whether higher deuterium content within tumors compared to healthy normal tissue, as a result of increased biosynthetic rates of the former, would allow distinct visualization of tumors via dMRI.

Deuterium incorporated into biomolecules during $^{2}H_2O$ labeling is detectable by dMRI

To detect deuterium-labeled metabolites *in vivo,* we tested several label-imaging protocols. We performed *in vivo* labeling on mice injected with HT-29 tumors followed by dMRI detection (Fig. 2a). For all protocols, one million HT-29 cells were injected subcutaneously on day 0. Labeling with $^{2}H_2O$ was performed on day -1 using an i.p. bolus to achieve ~5% TBW deuterium enrichment, and on day 0 using a second i.p. bolus to reach the 8% TBW enrichment, which was then maintained with drinking water (16% $^{2}H_2O$ in H_2O allows TBW to be maintained at ~8% $^{2}H_2O$ (v/v)[17]). Both hind limbs of the anaesthetized mouse, one leg bearing a tumor and the contralateral leg, were imaged using an MRI scanner equipped with a custom dual resonance ^{1}H-^{2}H coil (see Supplementary Fig. 2) 7 or 14 days post tumor cell injection (Fig. 2a). We also tested a protocol where the tumor cells were injected and allowed to grow *in vivo* for 7 days prior to initiation of labeling to ~8% $^{2}H_2O$ in TBW, with imaging performed on day 14. The latter schema was undertaken to test our ability to label and detect pre-existing tumors.

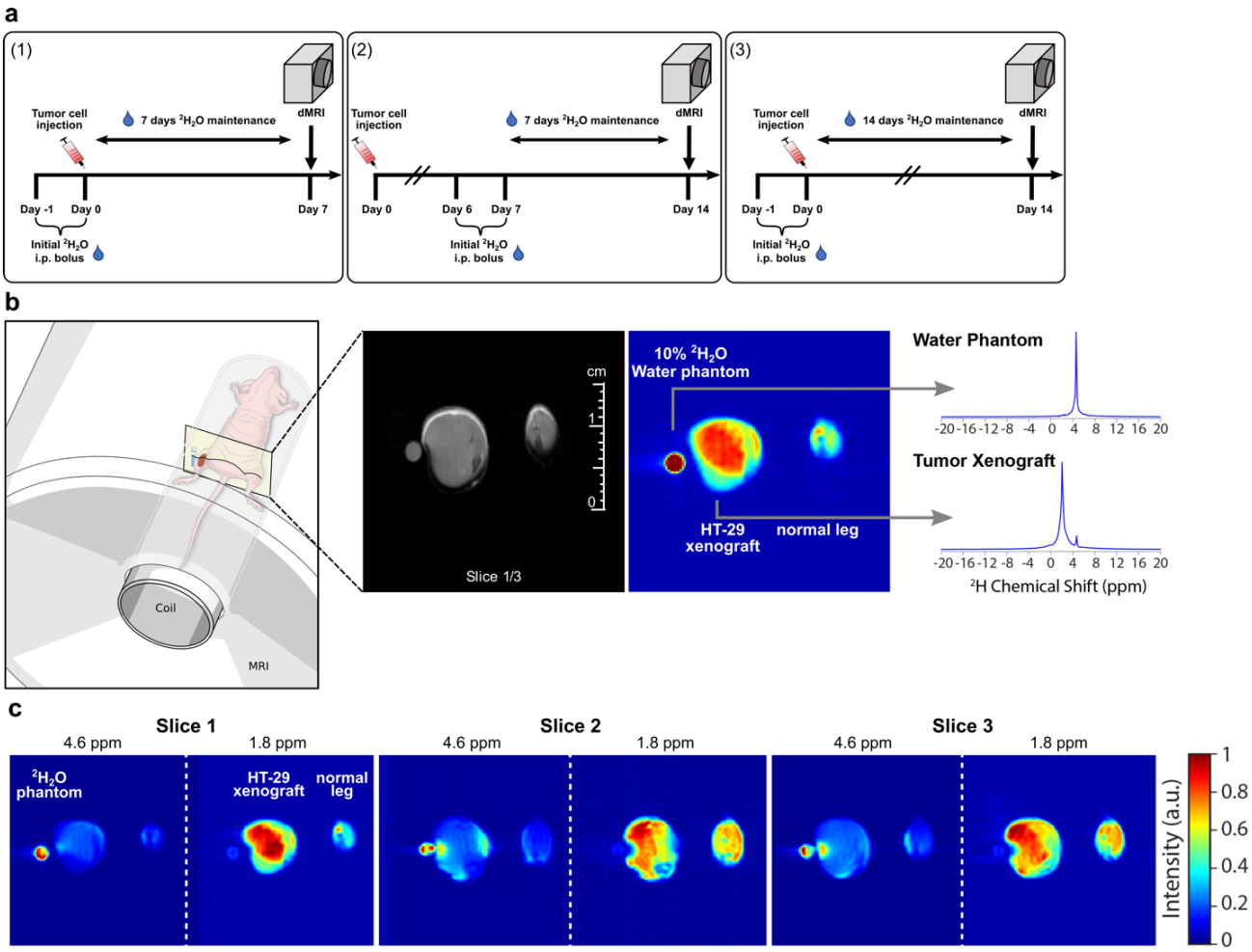

Figure 2: ^{2}H-MRI chemical shift imaging of xenografted HT-29 tumors in mice at 11.7T. a) *Labeling protocol for imaging experiments. Mice that underwent imaging were either labeled with two i.p. bolus injections (35 ml/kg 0.9% NaCl in 100% ^2H_2O) 24h apart on day -1 and 0 (1+3) or on day 6 and 7 (2) and were subsequently provided a 16% ^2H_2O maintenance dose in drinking water for 7 (1+2) or 14 days (3) after tumor implantation. Human HT-29 adenocarcinoma cells (1x10^6) were subcutaneously injected on day 0 into the right hind limb of athymic Foxn1^{nu} mice.* ***b)*** *Illustration of the imaging setup (left) with a representative deuterium image (right) along with the corresponding anatomical proton MRI image (center) for labeling protocol (3). Chemical shift imaging was used to acquire a 64 x 64 grid of deuterium spectra with each spectrum corresponding to a voxel 0.5 mm x 0.5 mm x 3 mm in size. The deuterium image was formed by summing across the entire spectra while the spectra corresponding to the individual voxels indicated are shown on the right (top, ^2H_2O phantom; bottom, tumor xenograft). The anatomical imaging was acquired using a spin-echo sequence with TR/TE = 500 ms/ 8ms and the same geometry as chemical shift imaging but with a matrix size of 128 x 128.* ***c)*** *Spectrally selective images for the mouse from (b) corresponding to the two major peaks at 4.6 ppm (^2H_2O chemical shift) and 1.8 ppm.*

Figure 2b shows a representative slice from a 3-slice, 64 x 64 image of deuterium spectra (voxel size 0.5 mm x 0.5 mm x 3 mm) showing the hind limbs of a female athymic mouse with the right leg bearing a relatively small (<1 cm, compared to the 3 mm reference vial) HT-29 tumor xenograft and the left leg serving as a control. The raw image was processed by applying our recently published de-noising algorithm that uses tensor decomposition to increase the deuterium signal-to-noise ratio (SNR)[32]. A 3-mm NMR capillary tube containing 10% ^2H_2O was placed near the left leg and served as a deuterium reference for the frequency of the water signal (left image). Figure

2b shows a slice from the deuterium image summed over all frequencies (right image) along with the corresponding T2-weighted anatomical MRI (center image) 14 days after tumor cell injection and concurrent deuterated water labeling to 8% TBW. Two major peaks can be detected in the deuterium spectra. The first is centered at 4.6 ppm near the expected frequency of the $^{1}H^{2}HO/^{2}H_2O$ water peak (top). There is a close correspondence between the anatomical MRI and the deuterium image at the water frequency, indicating background TBW deuterium enrichment is similar between the tumor-bearing limb and the unmanipulated limb (Fig. 2c). The remaining, non-water derived signal is characterized by an intense peak (mean SNR ~150) with a chemical shift of around 1.8 ppm (Fig. 2b, bottom spectrum) that is primarily, but not exclusively, observed in the tumor region. Figure 2c shows an example of all three slices acquired and separated into the two distinct frequencies, demonstrating that the tumor deuterium signal is not attributable to free $^{2}H_2O$. In all three slices, the deuterium signal intensity at 1.8 ppm is highest in the tumor bearing limb. The exact identity of the peak cannot be directly inferred from MRI, but the shift indicates that the peak likely originates from the resonance of alkyl groups taking into account possible B_0 distortion caused by proximity to the partially filled $^{2}H_2O$ phantom vial[33].

dMRI distinguishes tumors from normal tissue

Throughout the tested experimental schemas, we consistently observed a stronger deuterium signal at ~1.8 ppm in the tumor region compared to the contralateral limb (Fig. 3a). The degree of contrast, however, was dependent on both the length and timing of the labeling period (Fig. 3b). The strongest contrast (median=1.40, p= 0.02 on a per mouse basis, Wilcox's signed rank test), quantified as a ratio of the mean grey value between the HT-29-injected and normal leg, was observed after 14 days of tumor growth with labeling starting on the 6th day (labeling schema (2) in Fig. 2a, cyan squares in Figure 3b). Limiting both growth and labeling to the first 7 days (labeling schema (1) in Fig. 2a) led to negligible contrast (median=0.96, p=0.81). A similar trend was observed in an independent experiment performed on a 9.4 T MRI (Supplementary Fig. 3). Labeling for the full 14-day tumor growth period (labeling schema (3) in Fig. 2a) decreased contrast relative to starting at the 6-day midpoint (median=1.20, p=0.11). No significant difference in contrast was observed comparing the signal intensity at 4.6 ppm for any labeling protocol. Interestingly, while the MRI contrast was strongly dependent on the labeling period, the degree of deuterium labeling in both dA and in TBW was nearly independent of the labeling period (Fig. 3c, d).

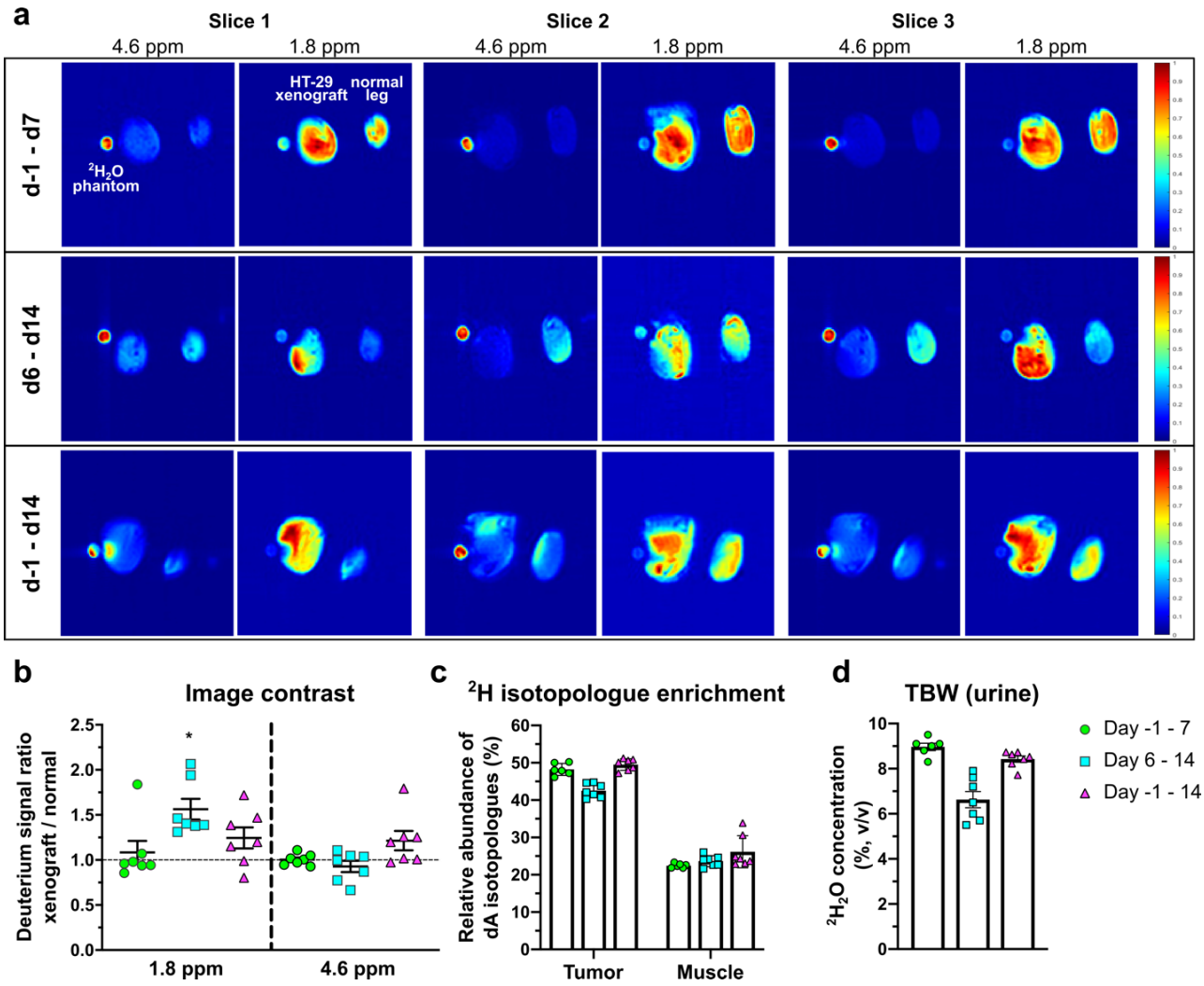

Figure 3: Comparison of different labeling strategies for dMRI detection of HT-29 tumors. a) *Representative images of the three labeling protocols shown as spectrally separated images for the 1.8 ppm and 4.8 ppm (water) peaks across three slices.* ***b)*** *Quantification of the contrast between tumor and control hind legs for the labeling schemas defined in Fig. 2a summed across the leg volume for the aliphatic (1.8 ppm) and water (4.6 ppm) signal regions. The leg area was defined as an ROI, the mean grey value was measured within and expressed as a ratio between the HT-29-injected and normal leg. Statistical analysis was performed using a Wilcoxon signed rank test against a hypothetical median of one, *=p<0.05, n=7 per group.* ***c)*** *Relative abundance of dA isotopologues after a 7-day or 14-day labeling period in tumor and muscle tissue (n=6-7 per group) analyzed via GC-MS.* ***d)*** *The ^2H_2O concentration in total body water was quantified using urine samples collected after 7 and 14 days of labeling via HS-GC-MS (n=6-7 per group).*

Discussion

In this study, we have explored the use of deuterium as a nonradioactive imaging label for the detection of tumors. We show that deuterated water administration results in sufficient deuterium MRI signal within xenografted HT-29 tumors to distinguish them from normal tissue via dMRI in a preclinical mouse model.

The first published use of deuterium in MRI was described in 1986[34]. Initial studies on dMRI showed that although deuterium only has a natural abundance of 0.015% and a gyromagnetic ratio that is 1/6th of a proton, therefore yielding less sensitivity relative to proton, other properties, such as its short T1 relaxation time which allows for quicker signal averaging, can compensate for the less favorable MRI-relevant factors[34]. It has since been used in animal models to visualize blood flow within a variety of tissues, including tumors[35-38]. In contrast to our approach, most studies used a single bolus injection of deuterated water to trace the deuterium signal in the organ of interest over a short time frame of minutes to hours. This enabled the visualization of blood flow and vasculature allowing the evaluation of tumor perfusion, but perfusion alone does not discriminate between healthy tissue and tumor. Continuous labeling with deuterium rather than administering a bolus of deuterium-labeled metabolite enabled us to enrich the tumor tissue with ^{2}H through biosynthesis of molecules incorporating ^{2}H. Unlike deuterium imaging following a single bolus injection before image acquisition, the background signal of $^{2}H_2O$ in TBW in our protocol had equilibrated with the TBW; i.e. we were not evaluating a perfusion difference but rather the accumulation of recently synthesized biomolecules within the tumor. We have used dA deuterium enrichment to demonstrate and quantify the degree of nucleotide labeling, which estimates other biosynthetic labeling with deuterium[26,27]. Incorporation of deuterium into other major classes of biomolecules, such as amino acids/proteins[18,23], triglycerides/lipids[39-41], glycolysis[42] and TCA cycle intermediates[43], has been demonstrated. Therefore, we infer that many biomolecules are labeled with deuterium, and likely at multiple sites (see Supplementary Fig. 1b) given the highly anabolic nature of proliferating tumor cells. In turn, multiple ^{2}H atoms on biomolecules being detected may enhance imaging sensitivity.

The water frequency-subtracted signal in our dMRI images had a chemical shift of ~1.8-2 ppm, which indicates that we are detecting alkyl groups abundant within fatty acids. A similar MRI signature was observed by others after continuous labeling of mice with deuterated water, further supporting this conclusion[44,45]. While fatty acids comprise a significant proportion of the cellular biomass, we cannot exclude the contribution of other ^{2}H-enriched biomolecules to the detected signal. For example, metabolomic analyses of proliferating (cancer) cells have shown that amino acids, such as glutamine/glutamate or alanine, are highly abundant and make up a considerable proportion of the cellular biomass[46-48].

By testing different labeling schemas, we found that labeling from day 6 – 14 provided the highest contrast between the tumor-injected leg and the contralateral control. During this time period, the tumor doubles in size, which results in high tumor deuterium enrichment and thus readily detectable tumor mass[49]. Similarly, the low imaging contrast that was observed when labeling was performed from day -1 to day 7 may be explained by the tumor being small compared to the rest of the leg and the entire leg being used as a region of interest to quantify contrast. Surprisingly, 14 days of $^{2}H_2O$ labeling did not yield an enhanced contrast compared to labeling from day 6 – 14. It

is possible that prolonged labeling with ^2H_2O reduces the contrast between the highly proliferative tumor and muscle in the contralateral limb. Although the muscle tissue showed no significant increase in isotopologue enrichment of dA after two weeks of labeling, other biomolecules that contribute to the imaging but are not related to cellular proliferation may enrich with deuterium over time. This was previously observed with long term ^2H_2O labeling of healthy tissues[50].

Since short-term intake of low-to-moderate concentrations of deuterium is generally considered safe for humans and long-term toxicity studies in animals have not shown any detrimental effects below 20% TBW enrichment[20,21,51,52], labeling cancer patients to 6-8% TBW may be safe and feasible. Nonetheless, since clinical studies involving deuterated water administration have so far only been performed at 1-2% TBW enrichment[53,54], future studies would need to either lower the targeted TBW enrichment or incorporate close monitoring of patients during the labeling period to evaluate for possible adverse side effects. One logistical consideration for targeting a lower TBW enrichment is the volume of a single-dose that can be given to a patient. According to Busch et. al, intake of more than 70 ml of 70% ^2H_2O as a single dose can induce nausea and vertigo[17]. Hence, achieving 6-8% TBW enrichment with this labeling approach would take more than a week despite a similar TBW level being easily undertaken in study animals. Given the strength of the observed dMRI signal in our preclinical study (overall mean SNR~150) and the signal gain achieved by post-acquisition processing (~24 fold), our immediate future plans include testing this labeling/imaging protocol at lower TBW enrichments and lower magnet field strengths that are more widely available for clinical imaging (i.e. 3 T).

The use of deuterium in MRI has recently been described in two studies using a deuterated glucose bolus in combination with MRI to image metabolically active brain tumors[13,14]. While the initial study was performed at ultra-high field strength (16.7 T), De Feyter et al. were able to image the uptake and metabolism of deuterated glucose by glioma tumors in rats and patients at 4 T, confirming the clinical relevance of deuterium as an MRI label. While the latter represents a promising approach for short-term labeling and imaging of metabolism, deuterated glucose is metabolized rapidly resulting in prompt loss of deuterium signal[32]. The spatial specificity for proliferating cells in combination with stable incorporation of deuterium and a robust SNR after image processing in our work provides an alternative approach. Additionally, such an approach would be preferable in clinical settings where a large bolus of glucose is contraindicated, e.g. in diabetic patients or patients receiving corticosteroids. From an implementation standpoint, deuterium MRI is inexpensive with regard to label and system set-up, is technically straightforward, and can be used to evaluate multiple anatomical regions.

In summary, we have demonstrated that ^2H_2O labeling leads to stable incorporation of deuterium into HT-29 tumor cells *in vivo*. This enabled us to establish a dMRI approach that can distinguish a growing tumor from quiescent tissue in a nonradioactive manner. We believe that this novel proliferation based labeling-imaging technique could provide an excellent addition to existing cancer imaging approaches, representing a valuable imaging option especially in settings where repetitive exposure to radioactivity is of concern.

Methods

Mice

Female athymic nude (Foxn1^{nu}) mice aged 10 – 12 weeks were supplied by the Frederick Cancer Research Center (Frederick, MD, USA). Mice were kept under a 12h/12h light-dark cycle with *ad libitum* access to food and water. All animal procedures were approved by the NCI Institutional Animal Use and Care Committee.

Cells

The human colorectal adenocarcinoma cell line HT-29 was purchased from ATCC (HTB-38) and the identity was confirmed using a panel of microsatellite markers (IDEXX Laboratories). HT-29 cells were cultured in RPMI 1640 supplemented with 10% fetal bovine serum, 100 U/ml penicillin, 100 µg/ml streptomycin and incubated at 5% CO_2 and 37 ˚C. On the day of tumor injection, HT-29 cells were spun down at 1000 rpm for 5 min, resuspended in PBS and 1×10^6 cultured cells were injected subcutaneously into the right proximal hind limb of the mouse. The contralateral hind limb of each mouse served as an intra-individual control, which did not receive a tumor cell injection.

Deuterium labeling

The dMRI studies were performed per the experimental schema described in Fig. 2, either 7 or 14 days after tumor cell implantation. For these imaging studies, a ^2H_2O level of ~8% in total body water (TBW) was targeted. The mice initially received two bolus injections (35 ml/kg body weight) containing NaCl (0.9%, w/v) in ^2H_2O (100%) 24 h apart, each bolus increasing the TBW enrichment by ~4%. Thereafter, the mice were provided drinking water containing 16% (v/v) ^2H_2O until imaging was performed[17]. Administration of 16% (v/v) ^2H_2O to maintain 8% ^2H_2O in TBW was necessary to account for the dilution of ^2H_2O by a factor of 0.3-0.4 due to the loss of ^2H_2O from respiration and excretion[17]. ^2H_2O dosing was either initiated the day prior to tumor cell injection or 6 days after as indicated in the figure legend. For the dose-escalation study, mice received 1-4 bolus injections within 7 days prior to tumor cell injection and were subsequently provided 8%, 16% and 32% ^2H_2O drinking water to achieve targeted concentrations of 4%, 8% or 16% ^2H_2O in TBW based on previous publications[17]. Regular drinking water served as a control (0% ^2H_2O).

Proton and deuterium magnetic resonance imaging (dMRI)

MRI experiments were performed on a 11.7 T (Magnex Scientific) or 9.4 T (Biospec 94/30) MRI equipped with a Bruker Advance III MRI console (Bruker-Biospin) and a custom, in-house built elliptical dual-resonance coil (^{1}H-^{2}H, Supplementary Fig. 2). The radiofrequency (RF) probes (coils) were used in transmit/receive mode within the MR system. Both, the ^{1}H saddle coil and the oval ^{2}H solenoidal coil were placed on a 3D-printed, oval-shaped former that was attached below a platform where the animal was staged. The hind legs of the mouse were placed side by side through an opening in the platform to the inside of the former. The ^{2}H coil wires (silver-plated 1.6 mm thick varnished copper) were tightly wound around the oval former and contain several in-line capacitors. The wires were attached to a standard tune/match circuit that transform its impedance to the 50 Ω characteristic impedance of the RF transmission line. The wires of the ^{1}H

coil were wrapped around the shell of the solenoidal coil at a distance and were independently mechanically supported. This saddle coil had two saddle shaped branches that were connected in parallel to a standard tune/match circuit for 50 Ω characteristic impedance RF transmission line. Both branches had in line capacitors and branch coupling capacitors to null undesired interaction of the two parallel branches. Homogeneity of both coils was tested using a tight fitting 3-D printed customized oval bottle that contained a mixture of saline enriched with ^{2}H.
Mice were anesthetized with isoflurane (4% for induction and 1.5% – 2.5% for maintenance in medical air, 500 ml/min). While anesthetized, the respiratory rate was monitored with a pressure transducer (SA Instruments Inc.) and maintained at 60 ± 10 breaths per minute. Core body temperature was also monitored using a nonmagnetic rectal temperature probe (FISO) and maintained at 36 ± 1°C using a circulating water-warming pad.

Immediately following anesthesia, both hind limbs were placed into the $^{1}H/^{2}H$ coil. A 3-mm diameter phantom tube 10% $^{2}H_2O$ in H_2O (v/v) was placed adjacent to the right hind limb and was included with each scan to serve as a deuterium reference signal.
For dMRI imaging, three 64 × 64 slices of 0.5 mm × 0.5 mm × 3 mm in size were acquired by chemical shift imaging without ^{1}H decoupling using standard linear k-space encoding with a 397 ms repetition time, 512 FID points, and a sweep width of 4,000 Hz using the described custom built elliptical dual-tuned $^{1}H/^{2}H$ coil. Due to difficulties in proper phase adjustment arising from the susceptibility artifact near the $^{2}H_2O$ glass tube, the spectra in each voxel were processed in magnitude mode. The images were then zero-filled to a final size of 128 × 128 × 3. The total scan time was 27 minutes.

To increase the sensitivity to the weak background $^{2}H_2O$ signal, a custom signal reduction algorithm was employed that takes advantage of the repeating structure of the data by decomposing the 4D image into a multilinear combination of vectors representing spectra and image columns and rows by low rank Tucker Decomposition, using 32 spectral vectors, 32 image vectors in each direction and all 3 slice vectors to reconstruct the original the 512 × 128 × 128 × 3 image[32]. Using this method, 92 ± 4% of the variance was captured in each scan, with the residual approximately corresponding to the noise level by visual analysis. Noise reduction was primarily used to detect the weaker $^{2}H_2O$ signal at 4.6 ppm - maps of the stronger metabolite signal at 1.8 ppm were similar in the presence and absence of noise reduction. The water peak from $^{1}H^{2}HO$ was set to 4.6 ppm relative to the DSS value, following a temperature correction to 37 °C[55]. The anatomical imaging was performed using the following parameters: spin-echo sequence, TR/TE = 500 ms/ 8ms, with the same geometry as chemical shift imaging but with a matrix size of 128 x 128.

To compare metabolism between tumor and non-tumor areas, a spectrally selective image was first formed by summing the 10 points (156 Hz) on either side of the two major peaks in the spectra after noise reduction. A region of interest was then drawn around the right and left leg for each of the three slices in ImageJ[56]. The mean greyscale value was tabulated for each region and a ratio between the signal intensity of the HT-29-injected and the normal leg was calculated for both spectrally selective images.

Urine/serum sample collection for HS-GC-NCI analysis
Urine or serum samples were collected from each mouse following the completion of dMRI image acquisition. As mice recovered from anesthesia on a heating plate, ~50 µl of urine was collected

on a sheet of parafilm upon spontaneous passage. The urine was immediately transferred to a plastic microcentrifuge tube. Serum was collected via mandibular or retroorbital bleed and allowed to clot for 30 min at room temperature. The samples were spun down at 2,655 x g (5417R, Eppendorf) and the supernatant was transferred to a new microcentrifuge tube. Urine and serum samples were stored at –20 °C until TBW $^{2}H_2O$ enrichment analysis using headspace gas chromatography–negative chemical ionization mass spectrometry (HS-GC-NCI-MS) was performed as previously published[27].

Tissue sample collection and preparation for GC-MS/MS enrichment analysis

To determine the isotopological enrichment of deuterium in the DNA base deoxyadenosine (dA), tissue samples from HT-29 tumors or anterior thigh muscle of the contralateral hind limb were excised immediately post-mortem after imaging and stored at -80 °C. Subsequently, we used a modified version of our validated GC-MS/MS method for analysis[26]. Briefly, after isolating DNA from mouse tissue samples using a tissue DNA extraction kit (Maxwell® 16, Promega), the purified DNA was incubated and hydrolyzed enzymatically (EpiQuik, Epigentek Group Inc.) to its nucleoside bases (e.g. dA, dT). The method employed solid phase extraction (Waters HLB) to extract and purify dA (unlabeled and deuterium labeled) from leg muscle and tumor tissue, with automated on-line methylation (derivatization) and rapid chromatographic analysis (~6 min) using an Agilent GC-MS/MS system (7890A GC, LTM Series II Fast GC Module, 7000C GC-MS/MS Triple Quadrupole, 7693 Autosampler and 7697A Headspace Sampler, all Agilent Technologies). The prepared samples were injected into the GC using the following conditions (1 µL pulsed split-less injection at 235 °C; component separation using low thermal mass DB-17MS column 15 m x 0.25 mm ID x 0.25 µm film with column oven temperature program from 50-320 °C at 120 °C/min). The MS utilized positive chemical ionization (PCI with isobutane reagent gas) and full scan mode (150 to 350 Da) to acquire MS data for evaluation.

As depicted in Supplementary Fig. 1c, MS overlays (normalized) of methylated dA and its isotopologues (e.g. dA M+1, dA M+2, dA M+3 etc.) depict the stable isotopes of ^{13}C, ^{15}N, ^{2}H, ^{18}O found naturally (i.e. ~23% background) in methylated dA and its isotopologues (left, contralateral leg muscle, control), as well as enrichment of ~27% deuterium (~50% minus natural isotopic background) into the DNA base dA of rapidly proliferating cells (HT-29 tumor, right).

Statistical analysis & software

For HS-GC-MS/MS operation, data acquisition and processing, we utilized a PC workstation with Agilent Masshunter Acquisition (B.07.06.2704), Quantitative (B.08.00) and Qualitative (B.07.00, Service Pack 1) software.

Data were analyzed and visualized using GraphPad Prism 8.0. All graphs represent the mean value ± SEM. Statistical analysis was performed as indicated in the figure legends with $p<0.05$ considered significant.

Acknowledgements

We thank Dr. Nobu Oshima for technical assistance with *in vivo* injection of HT-29 cells and Dr. Ehydel Castro for performing phlebotomy on study animals. We acknowledge Drs. Steve J. Dodd, Martin J. Lizak, and Kazutoshi Yamamoto for assisting with MRI scan acquisition. We thank Christopher Johns for assistance with tissue processing and editing of the manuscript. We acknowledge Dr. Charles Zhu for assistance with 3D MRI coil design. We thank Ethan Tyler and

Erena He, medical illustrators with NIH Medical Arts, for generating the drawing used in Figure 2. This was work was supported by NCI, NIH intramural funding.

Author contributions

NPB conceived the project, designed and performed imaging experiments, and collected samples from study animals. KS cultured and injected the tumor cells, performed MRI on study animals, and collected tumor samples post imaging. JRB processed and analyzed the MRI data. NM and KAW assisted with imaging experiments and collected urine samples. JCA, KAW, NM, and DEF processed samples post collection. DEF performed the mass spectrometric analysis. HM designed and built the MRI coils. MCK and REG provided input on experimental design. JCA, JRB, NPB, and DEF analyzed the data. JCA and NBP wrote the manuscript. All authors contributed to the editing of the manuscript.

Competing interests

NPB, DEF, NM, HM, MCK, and REG are inventors on a patent application related to this work, PCT/US2017/058886. Additionally, JRB, HM, MCK are inventors on patent application pertaining to the signal-to-noise reduction algorithm, PCT/US2018/018217.

References

1 Mason, B. R. *et al.* Current Status of MRI and PET in the NCCN Guidelines for Prostate Cancer. *J Natl Compr Canc Netw* **17**, 506-513 (2019).

2 Hagaman, M. G. NCCN Imaging Appropriate Use Criteria Compendium: An Overview. *J Adv Pract Oncol* **8**, 203-204 (2017).

3 Lim, J. S. *et al.* CT and PET in stomach cancer: preoperative staging and monitoring of response to therapy. *Radiographics* **26**, 143-156 (2006).

4 Tee, S. S. & Keshari, K. R. Novel Approaches to Imaging Tumor Metabolism. *Cancer J* **21**, 165-173 (2015).

5 Linet, M. S. *et al.* Cancer risks associated with external radiation from diagnostic imaging procedures. *CA Cancer J Clin* **62**, 75-100 (2012).

6 Schauer, D. A. & Linton, O. W. NCRP Report No. 160, Ionizing Radiation Exposure of the Population of the United States, medical exposure--are we doing less with more, and is there a role for health physicists? *Health Phys* **97**, 1-5 (2009).

7 Flavell, R. R. *et al.* Malignancies with Low Fluorodeoxyglucose Uptake at PET/CT: Pitfalls and Prognostic Importance: Resident and Fellow Education Feature. *Radiographics* **36**, 293-294 (2016).

8 Shreve, P. D., Anzai, Y. & Wahl, R. L. Pitfalls in oncologic diagnosis with FDG PET imaging: physiologic and benign variants. *Radiographics* **19**, 61-77; quiz 150-151 (1999).

9 Ardenkjaer-Larsen, J. H. On the present and future of dissolution-DNP. *J Magn Reson* **264**, 3-12 (2016).

10 Ntziachristos, V., Pleitez, M. A., Aime, S. & Brindle, K. M. Emerging Technologies to Image Tissue Metabolism. *Cell Metab* **29**, 518-538 (2019).

11 Zaccagna, F. *et al.* Hyperpolarized carbon-13 magnetic resonance spectroscopic imaging: a clinical tool for studying tumour metabolism. *Br J Radiol* **91**, 20170688 (2018).

12 Kurhanewicz, J. *et al.* Hyperpolarized (13)C MRI: Path to Clinical Translation in Oncology. *Neoplasia* **21**, 1-16 (2019).
13 De Feyter, H. M. *et al.* Deuterium metabolic imaging (DMI) for MRI-based 3D mapping of metabolism in vivo. *Sci Adv* **4**, eaat7314 (2018).
14 Lu, M., Zhu, X. H., Zhang, Y., Mateescu, G. & Chen, W. Quantitative assessment of brain glucose metabolic rates using in vivo deuterium magnetic resonance spectroscopy. *J Cereb Blood Flow Metab* **37**, 3518-3530 (2017).
15 Jain, M. *et al.* Metabolite profiling identifies a key role for glycine in rapid cancer cell proliferation. *Science* **336**, 1040-1044 (2012).
16 Lunt, S. Y. & Vander Heiden, M. G. Aerobic glycolysis: meeting the metabolic requirements of cell proliferation. *Annu Rev Cell Dev Biol* **27**, 441-464 (2011).
17 Busch, R., Neese, R. A., Awada, M., Hayes, G. M. & Hellerstein, M. K. Measurement of cell proliferation by heavy water labeling. *Nat Protoc* **2**, 3045-3057 (2007).
18 De Riva, A., Deery, M. J., McDonald, S., Lund, T. & Busch, R. Measurement of protein synthesis using heavy water labeling and peptide mass spectrometry: Discrimination between major histocompatibility complex allotypes. *Anal Biochem* **403**, 1-12 (2010).
19 Strawford, A., Antelo, F., Christiansen, M. & Hellerstein, M. K. Adipose tissue triglyceride turnover, de novo lipogenesis, and cell proliferation in humans measured with 2H2O. *Am J Physiol Endocrinol Metab* **286**, E577-588 (2004).
20 Jones, P. J. & Leatherdale, S. T. Stable isotopes in clinical research: safety reaffirmed. *Clin Sci (Lond)* **80**, 277-280 (1991).
21 Klein, P. D. & Klein, E. R. Stable isotopes: origins and safety. *J Clin Pharmacol* **26**, 378-382 (1986).
22 Buxbaum, N. P. *et al.* In vivo kinetics and nonradioactive imaging of rapidly proliferating cells in graft-versus-host disease. *JCI Insight* **2** (2017).
23 Busch, R. *et al.* Measurement of protein turnover rates by heavy water labeling of nonessential amino acids. *Biochim Biophys Acta* **1760**, 730-744 (2006).
24 Voogt, J. N. *et al.* Measurement of very low rates of cell proliferation by heavy water labeling of DNA and gas chromatography/pyrolysis/isotope ratio-mass spectrometric analysis. *Nat Protoc* **2**, 3058-3062 (2007).
25 Previs, S. F. *et al.* New methodologies for studying lipid synthesis and turnover: looking backwards to enable moving forwards. *Biochim Biophys Acta* **1842**, 402-413 (2014).
26 Farthing, D. E. *et al.* Sensitive GC-MS/MS method to measure deuterium labeled deoxyadenosine in DNA from limited mouse cell populations. *Anal Chem* **85**, 4613-4620 (2013).
27 Farthing, D. E. *et al.* Comparing DNA enrichment of proliferating cells following administration of different stable isotopes of heavy water. *Sci Rep* **7**, 4043 (2017).
28 Gerlinger, M. *et al.* Intratumor heterogeneity and branched evolution revealed by multiregion sequencing. *N Engl J Med* **366**, 883-892 (2012).
29 Cantor, J. R. & Sabatini, D. M. Cancer cell metabolism: one hallmark, many faces. *Cancer Discov* **2**, 881-898 (2012).
30 Griffin, J. L. & Shockcor, J. P. Metabolic profiles of cancer cells. *Nat Rev Cancer* **4**, 551-561 (2004).
31 Howe, F. A. *et al.* Metabolic profiles of human brain tumors using quantitative in vivo 1H magnetic resonance spectroscopy. *Magn Reson Med* **49**, 223-232 (2003).

32 Brender, J. R. *et al.* Dynamic Imaging of Glucose and Lactate Metabolism by (13)C-MRS without Hyperpolarization. *Sci Rep* **9**, 3410 (2019).

33 Delikatny, E. J., Chawla, S., Leung, D. J. & Poptani, H. MR-visible lipids and the tumor microenvironment. *NMR Biomed* **24**, 592-611 (2011).

34 Ewy, C. S., Babcock, E. E. & Ackerman, J. J. H. Deuterium nuclear magnetic resonance spin-imaging of D2O: A potential exogenous MRI label. *Magnetic Resonance Imaging* **4**, 407-411 (1986).

35 Ackerman, J. J., Ewy, C. S., Kim, S. G. & Shalwitz, R. A. Deuterium magnetic resonance in vivo: the measurement of blood flow and tissue perfusion. *Ann N Y Acad Sci* **508**, 89-98 (1987).

36 Mattiello, J. & Evelhoch, J. L. Relative volume-average murine tumor blood flow measurement via deuterium nuclear magnetic resonance spectroscopy. *Magn Reson Med* **18**, 320-334 (1991).

37 Kovar, D. A., Lewis, M. Z., River, J. N., Lipton, M. J. & Karczmar, G. S. In vivo imaging of extraction fraction of low molecular weight MR contrast agents and perfusion rate in rodent tumors. *Magn Reson Med* **38**, 259-268 (1997).

38 Bogin, L., Margalit, R., Ristau, H., Mispelter, J. & Degani, H. Parametric imaging of tumor perfusion with deuterium magnetic resonance imaging. *Microvasc Res* **64**, 104-115 (2002).

39 Turner, S. M. *et al.* Measurement of TG synthesis and turnover in vivo by 2H2O incorporation into the glycerol moiety and application of MIDA. *Am J Physiol Endocrinol Metab* **285**, E790-803 (2003).

40 Lee, W. N. *et al.* Measurement of fractional lipid synthesis using deuterated water (2H2O) and mass isotopomer analysis. *Am J Physiol* **266**, E372-383 (1994).

41 Diraison, F., Pachiaudi, C. & Beylot, M. In vivo measurement of plasma cholesterol and fatty acid synthesis with deuterated water: determination of the average number of deuterium atoms incorporated. *Metabolism* **45**, 817-821 (1996).

42 Landau, B. R. *et al.* Use of 2H2O for estimating rates of gluconeogenesis. Application to the fasted state. *J Clin Invest* **95**, 172-178 (1995).

43 Silva, A. M., Martins, F., Jones, J. G. & Carvalho, R. 2H2O incorporation into hepatic acetyl-CoA and de novo lipogenesis as measured by Krebs cycle-mediated 2H-enrichment of glutamate and glutamine. *Magn Reson Med* **66**, 1526-1530 (2011).

44 Brereton, I. M., Irving, M. G., Field, J. & Doddrell, D. M. Preliminary studies on the potential of in vivo deuterium NMR spectroscopy. *Biochem Biophys Res Commun* **137**, 579-584 (1986).

45 Kosenkov, A. V., Gulyaev, M.V., Lobyshev, V.I., Yusubalieva, G.M., Baklaushev, V.P. The Reversible Effect of Deuteration on Tissue Fluid and Biopolymers in Normal and Tumor Tissues of Mice. *Biophysics* **63**, 820-824 (2018).

46 Hensley, C. T., Wasti, A. T. & DeBerardinis, R. J. Glutamine and cancer: cell biology, physiology, and clinical opportunities. *J Clin Invest* **123**, 3678-3684 (2013).

47 Sheikh, K., Forster, J. & Nielsen, L. K. Modeling hybridoma cell metabolism using a generic genome-scale metabolic model of Mus musculus. *Biotechnol Prog* **21**, 112-121 (2005).

48 Hosios, A. M. *et al.* Amino Acids Rather than Glucose Account for the Majority of Cell Mass in Proliferating Mammalian Cells. *Dev Cell* **36**, 540-549 (2016).

49 Saito, K. *et al.* 13C-MR Spectroscopic Imaging with Hyperpolarized [1-13C]pyruvate Detects Early Response to Radiotherapy in SCC Tumors and HT-29 Tumors. *Clin Cancer Res* **21**, 5073-5081 (2015).

50 Müller, S. & Seelig, J. In vivo NMR imaging of deuterium. *Journal of Magnetic Resonance* **72**, 456-466 (1987).

51 Katz, J. J., Crespi, H. L., Czajka, D. M. & Finkel, A. J. Course of deuteriation and some physiological effects of deuterium in mice. *Am J Physiol* **203**, 907-913 (1962).

52 Hughes, A. M., Bennett, E. L. & Calvin, M. Production of Sterility in Mice by Deuterium Oxide. *Proc Natl Acad Sci U S A* **45**, 581-586 (1959).

53 Neese, R. A. *et al.* Measurement in vivo of proliferation rates of slow turnover cells by 2H2O labeling of the deoxyribose moiety of DNA. *Proc Natl Acad Sci U S A* **99**, 15345-15350 (2002).

54 Burger, J. A. *et al.* Leukemia cell proliferation and death in chronic lymphocytic leukemia patients on therapy with the BTK inhibitor ibrutinib. *JCI Insight* **2**, e89904 (2017).

55 Hoffman, R. E. Standardization of chemical shifts of TMS and solvent signals in NMR solvents. *Magn Reson Chem* **44**, 606-616 (2006).

56 Schneider, C. A., Rasband, W. S. & Eliceiri, K. W. NIH Image to ImageJ: 25 years of image analysis. *Nat Methods* **9**, 671-675 (2012).